# Novel surfactant self-assembly process generates multi-scale surface topographies for stem cell growth and differentiation

**Eric G. Xie[1,2], Colin A. Cook[1,2], Warren L. Grayson[1-3], Jason J. Benkoski[4]**

[1]*Translational Tissue Engineering Center, Johns Hopkins University, Baltimore MD, USA*
[2]*Department of Biomedical Engineering, Johns Hopkins University, Baltimore MD, USA*
[3]*Department of Material Sciences and Engineering, Johns Hopkins University, Baltimore MD, USA*
[4]*Johns Hopkins University Applied Physics Laboratory, Research and Exploratory Development Department, Laurel, MD, USA*

*Abstract*

Topographical features on a substrate can greatly influence stem cell fate through contact guidance. While the response of stem cells to topography at the nano-, micro-, and meso-scale has been studied extensively, little is known about the interplay of surface features acting simultaneously across multiple length scales. A limiting factor has been the availability of high throughput methods for probing the potentially unlimited parameter space. Herein we describe a facile method for rapidly generating a hierarchy of multi-scaled topographical features on polymer substrates via the self-assembly of surfactants at the monomer/water interface. Having previously assembled polydimethylsiloxane-diacrylate (PDMS-DA) into surfaces resembling multiple tissue morphologies, the current study refines this method to produce biocompatible substrates. To manage the large parameter space, we limit the scope of this study to surface features spanning nanometer (< 1 μm) and micrometer (1-50 μm) length scales, which arise both individually and in combination. Adipose-derived stem cells were plated onto five surface types and their morphology, proliferation, and osteogenic differentiation were assessed after non-inductive and osteogenic culture. We observed statistically significant differences in cellular responses to each surface. Among our observations, the increased osteogenesis of cells on surfaces with nano-scaled features superimposed over micro-scaled features suggests that such hierarchical surface structure mediates the osteogenic properties of a surface.

*Keywords*: *Fossilized liquid assembly; Self-assembly; Multi-scale topography; Adipose-derived stem cells; Bone tissue engineering; PDMS*.

*Available online at the Journal website: http://www.ache.org.rs/HI/*

SCIENTIFIC PAPER

**UDC 616.71:004:60:678.84**

*Hem. Ind.* **72** (2) 69–80 (2018)

## 1. INTRODUCTION

Several recent biomaterial studies have focused on the development of scaffolds with surface topographies that closely resemble that of human tissues [1-4]. The application of such structural cues has been shown to influence cellular behavior and tissue morphogenesis [5,6]. *In vitro* studies on artificial surfaces have demonstrated that structure alone significantly affects the organization of cells through contact guidance, and certain nano-patterns have reportedly induced differentiation in the absence of media components [7-13]. Nanotopography-directed osteogenesis in particular has been demonstrated in mesenchymal stem cells of adipose and bone marrow derivation, on polymer, biologic, and metallic surfaces [14-19]. A key limitation of tissue engineering scaffolds is the inability of conventional micro- and nanofabrication methods to match the complexity of the extracellular matrix (ECM). The ECM presents a hierarchy of topographical features from the nano- to macro-scale that template tissue growth. These

Correspondence: Warren L. Grayson, PhD, Johns Hopkins University, Department of Biomedical Engineering, Translational Tissue Engineering Center, 400 N. Broadway, Smith 5023, Baltimore MD 21231, U.S.A.
E-mail: wgrayson@jhmi.edu
Jason J. Benkoski, PhD, Johns Hopkins University Applied Physics Laboratory, Research and Exploratory Development Department, 11100 Johns Hopkins Rd, MS 21-N109, Laurel, MD 20723, U.S.A.
E-mail: jason.benkoski@jhuapl.edu
Paper received: 12 April 2017
Paper accepted: 18 December 2017
**https://doi.org/10.2298/HEMIND170508020X**

features occur with different diameters, spacing, orientations, persistence lengths, and size distributions. Complicating the topography is the fact that the surface features superimpose upon one another at different length scales. Unfortunately, the vast parameter space currently precludes a thorough, systematic investigation of multi-scale cell-surface interactions. Facile high throughput methods are required in order to reduce the number of experiments needed to explore this parameter space to a more manageable number. By creating a technique to rapidly generate topographies that superimpose surface features from the nano- to macro-scale, a better understanding of cell-topography interactions that occur simultaneously across multiple length scales can be exploited for bioactive material scaffold development.

Various methods can be employed to generate topographical structures on the surface of biomaterials. Commonly used are high-throughput methods such as plasma treatment and acid-base etching [20,21]. While effective for rapid generation of topographies, these methods suffer from limited control of feature geometry and poor consistency. Conventional photolithography, on the other hand, is precise, consistent, and provides direct control of geometry. However, its resolution is inherently limited to the wavelength of the exposure light, which is generally in the hundreds of nanometer range [22,23]. Additionally, despite being able to generate any two-dimensional (2D) patterns, photolithography produces topographies that are generally limited to prismatic structures on planar surfaces. For structures smaller than the wavelength of light, colloidal lithography can achieve feature sizes on the order of 50 nm [24,25]. It is somewhat defect-prone, though, as the patterns are developed through processes that thermodynamically favor defects. Electron-beam lithography (EBL) can produce defect-free nano-patterns with a similar level of control as photolithography, but pushes the maximum resolution even further to 11 nm [26]. Unfortunately, long write times make it impractical for many cell studies.

Our laboratory has previously developed a novel self-assembly technique (dubbed Fossilized Liquid Assembly; FLA), which, in a single step, superimposes topographical patterns ranging from tens of nanometers to several millimeters in size [27, 28]. The features primarily consist of bumps, pores, and ridges, which may superimpose upon each other with up to seven levels of hierarchy. Quantitative image analysis revealed that the surfaces are generally multi-fractals. In addition, they differ from most photolithographic patterns in terms of randomness and the breadth of the feature size distribution. Few synthetic techniques combine multi-fractal morphology, multiple levels of hierarchy, randomness, wide size distributions, and the main structural motifs of the ECM.

Sample preparation consists of dissolving a nonionic surfactant in polymer, coating the polymer on a solid substrate, and then immersing it in water. The high interfacial tension drives the segregation of surfactants dissolved in the oil phase to the boundary layer where they deform the liquid/liquid interface, simultaneously giving rise to nano-, micro-, and macro-scale features. Then cross-linking the oil phase into a solid polymer preserves a “snapshot” of the self-assembly at the instant of UV exposure. Varying surfactant structure, concentration, self-assembly time, and film thickness creates distinct surface morphologies. Relative to lithography, FLA has the advantage of cost, speed, and simplicity. The entire process takes less than five minutes and can be used to create gradient surfaces. These include gradients in thickness, surface features, levels of hierarchy and surfactant concentrations [29].

Compared to chemical etching methods, FLA offers much greater control and a wider variety of morphologies and captures the complexity, disorder, fractal geometry, and hierarchical organization of biological materials, and the ECM in particular. FLA has been demonstrated on methacrylates, styrenes, fluoroacrylates, and silicones. The PDMS-DA used in this study contains ester-ether bonds that slowly hydrolyze in water. The hydrolytic degradation rate can be increased up to 10 times through the introduction of thiol-acrylate bonds [30]. The byproducts of PDMS-DA degradation may hold key advantages in that they have a smaller inflammatory effect due to their low acidity [31] and ability to be easily cleared by the body [32] limiting bioaccumulation [33-36].

This study used poly (dimethylsiloxane-diacrylate) (PDMS-DA), which can form surfaces that bear strong topographic resemblances to various tissue types [29]. Combined with its biocompatibility and the ability to tune its elastic modulus to match native tissue properties, PDMS-DA is a promising model system for probing cell-surface interactions [37]. Moreover, the goal of this study is to evaluate the ability of this novel technique for generating topographical patterns to modify cellular responses to materials. We investigated the interplay among the different levels of hierarchy that act simultaneously over subcellular (< 1 μm), cellular (1-50 μm), and intercellular length scales (>50 μm) and probed the impact of multi-scale interactions to influence adipose-derived stem cells (ASCs) morphology and behavior. We quantitatively characterized the surface features generated by five distinct surfactants where the concentration, self-assembly time and film thickness were specified *a priori*. Human ASCs were cultured on the five distinct PDMS-DA surfaces as well as on a flat, control surface. We observed five very distinct sets of surface features and found that these could elicit differences in human ASC morphology, proliferation, and osteogenic differentiation. These findings suggest that there is potential for using this approach to modulate cellular responses to biomaterials.

## 2. MATERIALS AND METHODS

### 2.1. Reagents

All reagents were purchased from Sigma Aldrich and used without further purification unless otherwise noted. Bis(2,4,6-trimethylbenzyol)-phenylphosphine oxide (Irgagure 819, Ciba Chemicals, Switzerland), (3-acryloxy-2-hydroxypropoxy propyl) terminated polydimethylsiloxane (PDMS-DA, Gelest, Inc., 110 cSt viscosity, 7500 g/mol), polyoxyethylene (10) oleyl ether (C18E10), polyoxyethylene (2) oleyl ether (C18E2), polyoxyethylene (2) cetyl ether (C16E2), polyoxyethylene (4) dodecyl ether (C12E4), polyoxyethylene (2) hexyl ether (C6E2), phosphate-buffered saline (PBS), fetal bovine serum (FBS, Atlanta Biologics, USA). The hydrophile-lipophile balance (HLB) values of the five surfactants are provided in **Table I**.

*Table 1. HLB Values of Surfactants used in this study*

| Surfactant | C6E2 | C12E4 | C16E2 | C18E2 | C18E10 |
|---|---|---|---|---|---|
| HLB Value | 10.2 | 10.2 | 5.6 | 5.2 | 12.7 |

### 2.2. PDMS surfaces

Samples were prepared by first dissolving 1 % w/w Irgacure 819 in PDMS-DA by stirring at 60°C for one hour. Next, a surfactant was dissolved in the mixture at 10 % w/w. These were linear nonionic surfactants of the form CiEj, where i refers to the number of carbons in the aliphatic tail, and j refers to the number of repeat units in the polyethylene glycol head group. Five surfactants were tested in all: C6E2, C12E4, C16E2, C18E2, and C18E10. The mixtures were spin-coated on 15 mm-diameter glass coverslips at 6600 RPM for 5 sec to create the desired film thickness. The coated coverslips were attached to the back of a Petri dish and inverted onto water, as shown in **Fig. 1**. Self-assembly of the surfactants at the PDMS-DA/water interface resulted in unique and consistent topographies. The systems were allowed to self-assemble for 30 sec before being flash-cured with UV light (80 W system comprising two UV-B bulbs with 7080 W/m$^2$ at the PDMS/water interface). The flat control surface was created by using PDMS/initiator mixture without surfactant and eliminating the time allowed for self-assembly, beginning UV exposure upon contact with the water. Once the polymer solidified, the coated coverslips were removed from water and dried. They were then visually inspected using a Toshiba TM3000 tabletop scanning electron microscope (SEM). For quantitative topographical analysis, a Zeta Instruments Zeta-20 optical profilometer recorded the 3D height profile at a 100x magnification. Prior to cell seeding, the surfaces underwent a series of graded ethanol washes (70 %, 95 %, 100 %) for 12 h each to leach the cytotoxic photo-initiator and excess surfactant. Although the samples are referred to by the surfactant used to generate the surface topography, the surfactants were removed prior to cell exposure, leaving behind pure PDMS-DA. Samples were subsequently rinsed in phosphate-buffered saline (PBS). Finally, the surfaces were soaked in PBS containing 10 % fetal bovine serum (FBS, Atlanta Biologics, USA) for 24 h in order to coat the surface with proteins to facilitate cell attachment.

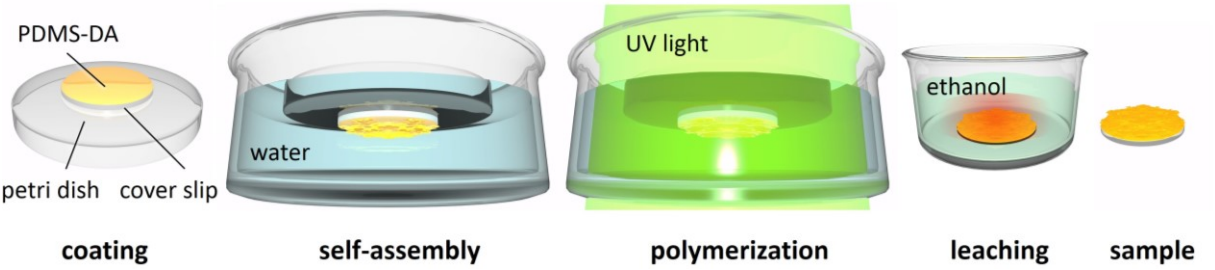


*Figure 1. From left to right, PDMS-DA-coated cover slips were attached to the back of a Petri dish, inverted, and floated in water. After allowing 60 s for self-assembly to take place, the samples were irradiated with UV light to solidify the PDMS-DA. The samples were removed from water, soaked in ethanol to leach out photo-initiator and excess surfactant, rinsed, and dried.*

### 2.3. ASC isolation and culture

Humans ASCs were a kind gift of Dr. Jeffrey Gimble. The ASCs were isolated under an Institutional Review Board approved protocol according to published methods [24]. For expansion, ASCs were thawed and cultured in expansion medium: high glucose DMEM (GIBCO Invitrogen, USA) with 10 % fetal bovine serum (FBS; Atlanta Biologicals), 1 % penicillin/streptomycin (GIBCO Invitrogen), and 1 ng/ml bFGF (PeproTech, USA). Cells from a single donor were used at passage four for all experiments. ASCs were seeded onto the prepared surfaces at 5,000 cells/cm$^2$ and cultured in 500 µl of the appropriate media. Cells were incubated at 37 °C, 5 % $CO_2$, and media was changed thrice weekly. To induce osteogenic differentiation, cells were cultured in osteogenic media (OM), which comprised of high glucose

DMEM with 10 % fetal bovine serum and 1 % penicillin/streptomycin with additional components 10 mM beta-glycerophosphate (Sigma, USA), 50 µM L-ascorbic acid-2-phosphate (Sigma), and 10 nM dexamethasone (Sigma). Samples were harvested at Day 0, 1, 4, and 7 for the proliferation experiments, and Day 21 for the osteogenic differentiation experiments.

**2.4. Scanning electron microscopy**

To examine cell morphology, cellularized surfaces were fixed in 3.7 % formaldehyde in PBS at 4 °C for 16 h. The samples were then washed thoroughly for 5 min in PBS followed by 10 min in deionized water before being frozen at -20 °C. Dehydration was accomplished by lyophilization of the frozen samples. Samples were then sputter coated with platinum before examination with scanning electron microscopy (JEOL 6700F) at 15KV. The images were also used to quantitatively verify the feature sizes reported from optical profilometry. This was performed at the day 1 time point so as to be able to identify individual cells' morphology before confluence or near-confluence.

**2.5. Optical profilometry**

In order to visualize the surfaces in 3D, optical profilometry (Zeta Instruments Zeta-20) was used to record a height profile at 100x magnification. This profile was then used for quantitative topographic analysis, yielding feature size in planar and height dimensions. Calculated from the height distributions were the root-mean-square (RMS) surface roughness (width of the height distribution), skewness (symmetry of the height distribution), and kurtosis (curvature of the height distribution). The root-mean-square roughness measures the degree of deviation from the midplane of the surface and captures the average height and depth of features but not their spacing. Positive kurtosis values indicate a slightly sharper peak and fatter tails relative to a Gaussian, whereas negative values indicate a rounded peak with short tails. Positive skewness values signify that the largest deviations from the mid-plane are protrusions, and negative values indicate that the largest features are depressions.

**2.6. Cell proliferation**

DNA content as a measure of cell number has been established as a surrogate for proliferation in a number of studies [38-41]. DNA content of the cultures was assessed using the Picogreen assay. ASCs were grown on the surfaces in 24-well plates. Upon harvest, cells were treated with 250 µl of lysis buffer comprised of 0.1 % Triton X-100, 1 mM EDTA, 10 mM Tris, 0.1 mg/mL proteinase K (Sigma). The samples were stored frozen at -20 °C. Immediately preceding analysis, samples were incubated at 50 °C for 16 h. DNA content was then determined using the Quant-It PicoGreen fluorescent quantitation kit (Molecular Probes, Thermofisher Scientific, USA). Samples were added in duplicate to a 96-well plate at a 1:1 dilution with Tris/EDTA buffer. PicoGreen dye diluted to 1:200 with Tris/EDTA was added at 100 µl per well. The plate was then read (excitation 485 nm, emission 530 nm) and DNA content was determined by comparison to standard samples. DNA content was evaluated at Days 0, 1, 4, and 7 for ASCs in growth medium and at Day 21 for ASCs undergoing osteogenic differentiation. The earlier time points were needed to show statistical differences in proliferation, whereas by latter time points, DNA content became roughly the same on all surfaces due to contact inhibition and was instead used for normalizing calcium mineralization.

**2.7. Calcium quantification**

To provide a benchmark for functional outcomes of our surfaces as indicated by literature [42-44], calcium deposition was evaluated for the osteogenic differentiation study at 21 days, as calcium deposition at earlier time points was negligible. Samples were separate from those used in the DNA assay and were harvested with 250 µl of 0.5 N HCl. To dissolve mineralized calcium, the samples were kept in the 0.5 N HCl at 4 °C for 16 h with agitation. After centrifuging the sample to pelletize cellular debris, calcium content was quantified from the sample supernatants using the colorimetric Calcium LiquiColor Test (Stanbio, Block Scientific, USA). Supernatant was added in duplicate to a 96-well plate at a 1:1 dilution (0.5 µl sample, 0.5 µl 0.5 N HCl), following which the colorimetric kit components were added. The plate was then read and calcium content determined from reference values.

**2.8. Phalloidin/DAPI**

Cellularized surfaces were fixed in 3.7 % formaldehyde in PBS at 4 °C for 16 h at Day 1. Samples were permeabilized with 500 µl of 0.2 % Triton-X in PBS for 10 min, and then washed in PBS for 5 min. Blocking was completed by incubating the samples in 500 µl of 10 % FBS in PBS for 30 minutes. Samples were then incubated with actin-staining phalloidin-TRITC (1:40, Sigma) for one hour. Following three washes in PBS, cell nuclei were stained with DAPI (1:2000, Sigma, USA) for five minutes. Samples were then mounted and imaged using a Zeiss Axio Observer inverted fluorescence microscope.

### 2.9. Quantitative image analysis

Morphological measurements of immunostaining were completed using Image J software (NIH). Thresholding was applied to fluorescent images from Day 1 of the proliferation study to isolate the cells. In order to determine the average and variance of cell area, counting and analysis was automatically performed using masks around individual cells. The area covered by cells was averaged from two random view fields per sample and two samples per surface.

### 2.10. Statistical analysis

Quantitative results are expressed as means +/- standard error. All experiments were conducted in triplicate (n = 3). Multi-group comparisons were determined by one-way analysis of variance (ANOVA) with the Dunnett's test for post-hoc analysis. Dunnett's test is a modified Student's t-test that allows multiple pair-wise comparisons of various experimental groups to a single control. Significance levels are denoted as *p<0.05, **p<0.01, and ***p<0.001.

## 3 RESULTS

### 3.1. Characterization of PDMS-DA surfaces

The different surfactants used in this study induced the formation of highly variable surface topographies on the PDMS-DA. SEM imaging demonstrated distinct but consistent surface features on the micron and sub-micron length scales (Fig. 2). Optical profilometry indicated that the heights of these features varied greatly based on surfactant type. For example, the surface of C18E2 consists of submicron ridges (average 300 nm in diameter and 40 nm in height) with no micron-scale features. Conversely, C12E4 possessed micron-scaled topographies with steep ridges ranging from 20 – 30 µm in height and width. The porous features of C18E10 were distinctly bimodal. One group of pores averaged 1.5 µm in depth and diameter while the other group had average measurements of 20 – 30 µm. Finally, the C6E2 and C16E2 samples included hierarchies of sub-micron-sized features superimposed on structures that were micrometer length scales. For example, there were nanometer-sized bumps on the C16E2 samples superimposed on 7 – 8 µm pores causing it to resemble a combination of the features on the C18E2 and C18E10 samples. Meanwhile, the C6E2 sample had nano-scale bumps on 2 – 3 µm ridges.

Taken together, these morphologies probe three distinct aspects of surface morphology: structural motif, hierarchical level, and size distribution. In terms of structural motif, three are represented, bumps, ridges, and pores. They are sometimes presented in combination. Since the film thickness was relatively thin, the number of hierarchical levels is limited to one or two. Finally, the size distributions followed either a unimodal or bimodal distribution. The latter is especially important to compare with the hierarchically structured surfaces. Thus one can distinguish between effects caused by having two different length scales present side by side versus the superposition of two different length scales. The different morphological characteristics of the samples in Figure 2 are summarized in Table 2.

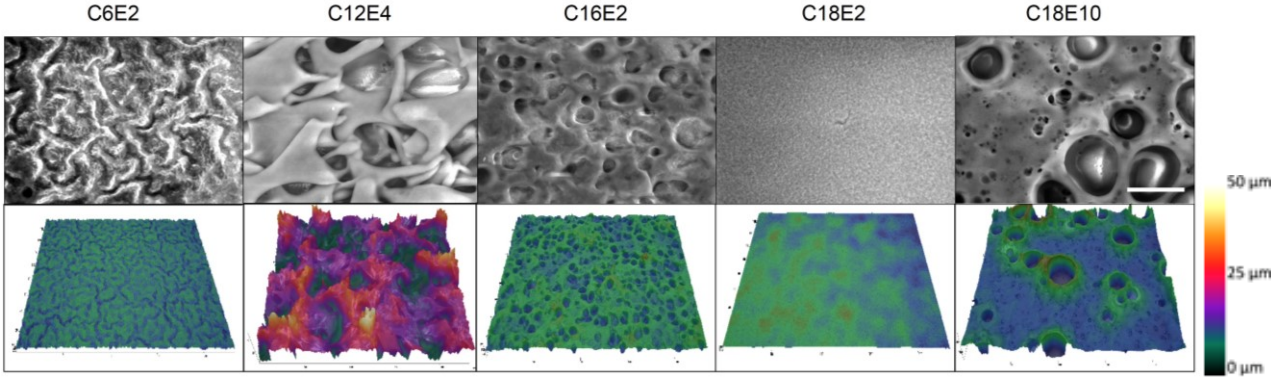


*Figure 2. (**Top row**): SEM images of topographical structure of PDMS surfaces fabricated by FLA with different surfactants at 10 % w/w (Mag = 2000X; scale bar = 30 µm). (**Bottom row**): 3D representations of optical profilometry images with FOV of 233x175 µm. The false color scale indicates height from blue at 0 µm, green at 12 µm, red at 50 µm, yellow at 40 µm, and white at 50 µm.*

*Table 2. Summary of morphological characteristics found on each sample surface*

| Sample | C6E2 | C12E4 | C16E2 | C18E2 | C18E10 |
|---|---|---|---|---|---|
| **Structural Motif** | Ridges and bumps | Ridges | Ridges and pores | Ridges | Pores |
| **Levels of Hierarchy** | 2 | 1 | 2 | 1 | 1 |
| **Size Distribution** | Unimodal, 100 nm bumps on 3 µm ridges | Unimodal, 30 µm ridges | Unimodal, 100 nm bumps on 8 µm pores | Unimodal, 300 nm ridges | Bimodal, 1 and 30 µm pores |

Quantitative characterization of these surface features was used to confirm qualitative observations (Fig. 3). The roughness of each surface was measured in microns as the root-mean-square of the heights of features on the surfaces. The roughest surface was C12E4 (5.94 ± 0.44 μm) and the values gradually decreased from C18E10 (3.82 ± 0.49 μm), C16E2 (1.30 ± 0.23 μm), C6E2 (0.46 ± 0.01 μm), and C18E2 (0.18 ± 0.06 μm) (Table 3). The dimensionless values of skewness and kurtosis were also included to more precisely describe the surface structure for each group. Skewness was small and negative for all samples, indicating that the surfaces were largely symmetric about the mid-plane, and that the largest deviations were deep depressions rather than tall protrusions. In order of decreasing skewness, the samples ranked C16E2, C6E2, C18E10, C18E2, and C12E4. Kurtosis was small and positive for all samples, indicating that the surfaces had a more distinct mid-plane relative to a random Gaussian distribution. In order of decreasing kurtosis, the samples ranked C12E4, C18E10, C16E2, C18E2, and C6E2 (Fig. 3).

### 3.2. ASC morphology

Fluorescent images of phalloidin-stained cells at Day 1 demonstrated that ASCs adopted distinct morphologies on the various surfaces (Fig. 4). The actin cytoskeletons as well as the overall shape of the cells were clearly observed on both experimental and control surfaces. Cells on the C18E2, C18E10, and flat surfaces displayed well-defined actin filament fibers. In contrast, the staining of the cytoskeletal fibers of ASCs grown on C6E2, C12E4, and C16E2 appeared more diffuse. The overall cell morphology was also distinctly different between surfaces. Increased filipodia-like cell protrusions and reduced cell spreading were observed on C6E2, C12E4, and C16E2 surfaces compared to cells cultured on the control (flat) surfaces via fluorescent stains and SEM images (Fig. 4). In contrast, increased cell spreading was observed on the C18E2 surface. Measurements of cell area from fluorescent images correlated with these findings.

*Table 3: RMS roughness of individual surfaces*

| Surface | RMS roughness, μm |
|---|---|
| **C6E2** | 0.46 ± 0.01 |
| **C12E4** | 5.94 ± 0.44 |
| **C16E2** | 1.30 ± 0.23 |
| **C18E2** | 0.18 ± 0.06 |
| **C18E10** | 3.82 ± 0.49 |

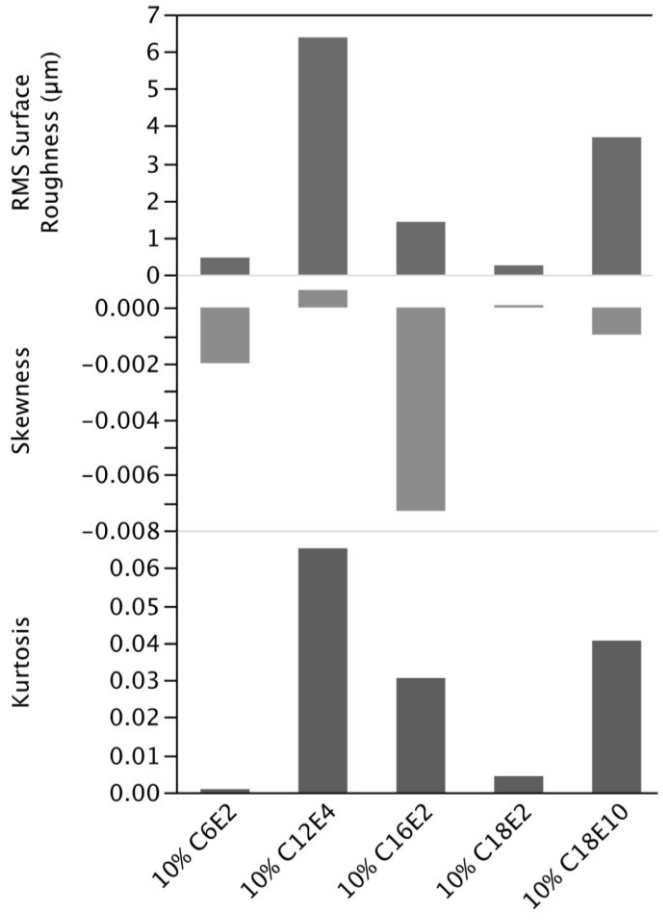


***Figure 3.*** *Characterization of FLA surfaces. Root mean square roughness, skewness, and kurtosis plotted for each sample type.*

### 3.3. ASC proliferation

ASC proliferation was quantified by measuring the total DNA content of each sample. In the day 0 samples, taken four hours after seeding, there were no measurable differences across surfaces, indicating that surface features did not affect initial cellular adhesion (Fig. 5A). However, measurements of DNA content at subsequent time-points indicated that ASC proliferation was affected by the surfaces. The DNA content of C16E2 was similar to the flat control throughout. Cells grown on C18E2 mostly followed the same pattern, but the cell number was slightly higher than control at day 7. In contrast, proliferation on C12E4 was consistently lower than the flat control. It was nearly 40 % at day 4, though the difference was much smaller at day 7 when DNA levels were 92 % of that of the flat surface. Proliferation on C18E10 was also decreased relative to the control at days 1 and 4, but was similar by day 7. Finally, the proliferation of C6E2 was lower than the control at day 1, no different at day 4, and higher at day 7. These results agreed with observations of live/dead stained images from samples at identical time points (not shown). The DNA content at day 7 was considered to be representative of confluence on the surfaces. Plotting DNA content at day 7 against the RMS surface roughness, demonstrated a potential correlation between roughness and proliferation (Fig. 5B).

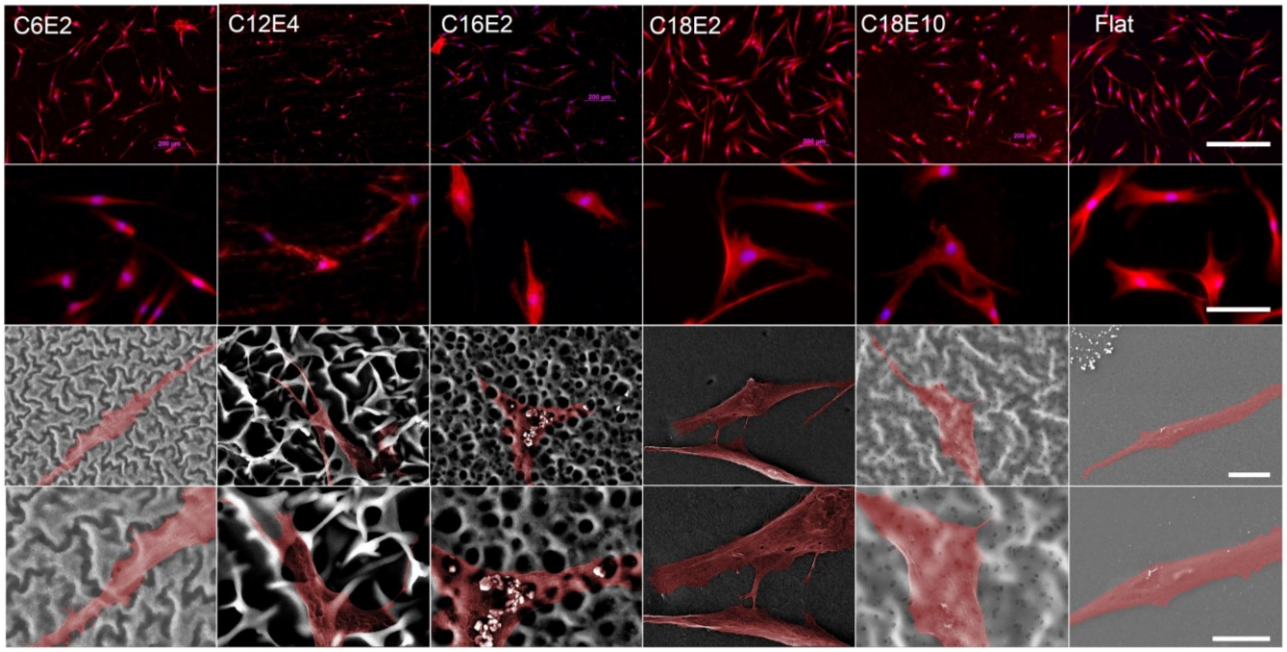


*Figure 4. Morphology of ASCs on FLA surfaces at Day 1. (**A**) Top two rows show actin cytoskeletons stained with phalloidin (red) and DAPI (blue) for ASCs. The bottom two rows show SEM images with ASCs pseudo-colored red. From top to bottom, scale bars = 400 µm, 100 µm, 30 µm, 20 µm. **(B)** Cell area plotted for each sample type. (Statistical significance indicated relative to flat samples. Significance levels are denoted as ***p<0.001, and ****p<0.0001.)*

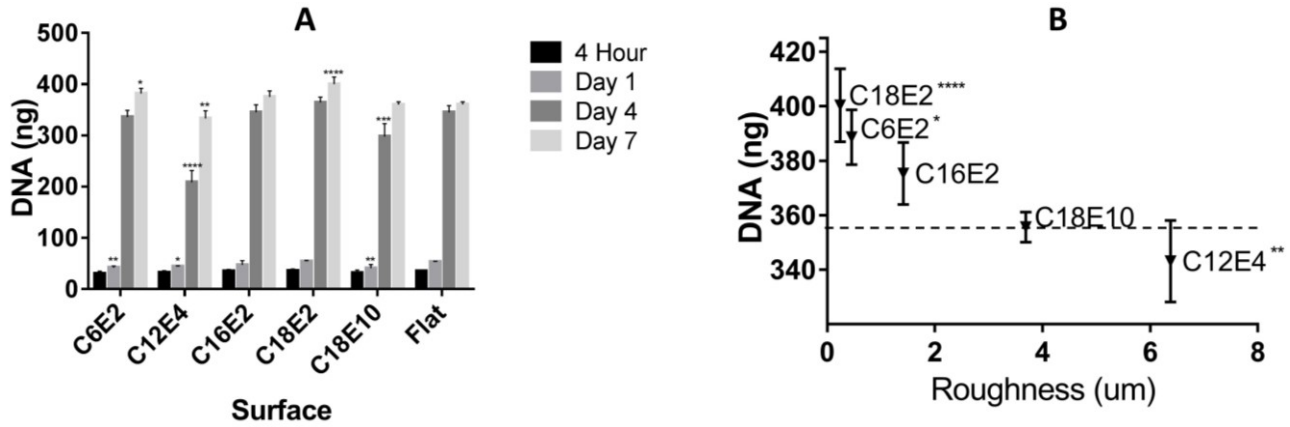


*Figure 5. **Effect** of topography on ASC proliferation. (**A**) Quantification of DNA content from cells harvested at various time points. (Statistical significance indicated relative to flat samples at the same time point) (**B**) Plot of DNA content versus RMS surface roughness at Day 7. Dashed horizontal line indicates DNA content of cells grown on flat surfaces. Solid line is best-fit with $R^2$=0.921. Significance levels are denoted as *p<0.05, **p<0.01, ***p<0.001, and ****p<0.0001.*

### 3.4. Osteogenic differentiation of ASCs

ASC osteogenic differentiation was quantified as the calcium deposition per DNA content of each surface after 21 days (Fig. 6A). Proliferation across surfaces was statistically identical with the exception of C6E2, which was 9 % lower than the flat control. Total calcium deposition was notably higher on C6E2, C12E4, and C16E2 compared to the control, with a roughly 30 % increase in normalized mineral deposition relative to the control surface. There was no measurable difference in mineral deposition of C18E2 or C18E10 relative to the flat control. In contrast to the DNA content, the normalized calcium concentration showed no clear trends with respect to surface roughness (Fig. 6B). Cell area measurements were quantified from phalloidin/DAPI images at day 1. The cell areas on day 1 on C6E2, C12E4, and C16E2 (the surfaces that induced increased mineral deposition) were significantly lower (1810 µm$^2$/cell) relative to the flat surfaces as well as C18E2 and C18E10 (3220 µm$^2$/cell) (Fig. 6C). These differences are shown in the comparison of mineral deposition on Day 21 and measured cell area on Day 1 on the respective surfaces (Fig. 6D).

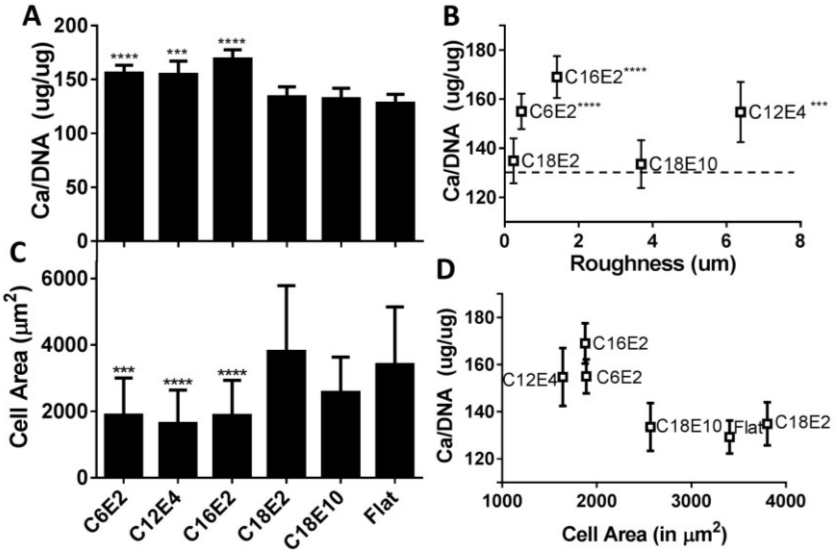


***Figure 6.*** *Effect of topography on ASC mineral deposition (**A**) The Ca/DNA concentration is plotted for each surface type. (Statistical significance indicated relative to flat samples) (**B**) The normalized Ca/DNA concentration plotted against the RMS surface roughness indicates there is no correlation between these two parameters. Dashed horizontal line indicates Ca/DNA content of cells grown on flat surfaces. (**C**) Total Ca per well without normalization. (**D**) When plotted versus cell area, the normalized Ca/DNA concentration shows an inverse relationship with cell area.*

## 4. DISCUSSION

The aims of this study were to refine the use of FLA technique in generating cytocompatible surfaces with biomimetic topographies and to explore the potential of these surfaces for culturing cells. Specifically, we probed the surfaces using ASCs and determined the effects of topography on ostogenesis. Previous studies showed that FLA offers wide-ranging control of morphology through four primary processing parameters: surfactant type, surfactant concentration, self-assembly time, and film thickness [33]. Each combination of surfactant and concentration defines a unique structural motif, which may include pores, bumps, and ridges. Film thickness and self-assembly time affect gradual changes in the topographical structure. Increasing the film thickness increases the dominant length scale of the surface morphology and the number of hierarchical levels at larger length scales, resulting in an amplification of surface roughness. Increasing the assembly time increases the number of hierarchical levels at smaller length scales, affecting the specific surface area. To make the set of experiments more manageable, we restricted the range of features to cellular and sub-cellular length scales by using only thin PDMS-DA films (7.41 ± 0.03 μm), which precluded the growth of larger features. To further focus the study, the number of groups was limited by employing a single self-assembly time (30 s) and surfactant concentration (10 % w/w). The effects of changes in surface chemistry were minimized by thoroughly removing the surfactants through graded ethanol washes.

Surfactant type was the only processing parameter varied for the study. This generated a variety of structural morphologies that included nanoscale features only, microscale features only, or a combination of the two. For example, C18E2 contained sub-cellular ridges with no micro-scale features. Conversely, the C18E10 samples had only microscopic pores with no sub-micron features. C12E4 also lacked sub-micron features, but its microstructure consists of thin protrusions. C16E2 and C6E2 samples were more hierarchical in structure. For C16E2, sub-micron bumps were superimposed over microscopic pores while C6E2 had submicron bumps superimposed over microscopic ridges. C16E2 combines structural characteristics of C18E2 and C18E10, while C6E2 combines features of C18E2 and C12E4.

The effect of surfactant structure on surface morphology is difficult to predict *a priori*, but two general rules apply to linear nonionic surfactants of the form CiEj [33]. Surfactants with a hydrophilic-lipophilic balance number (HLB) greater than 10 tend to form bumps due to their positive spontaneous curvature, and surfactants with HLB numbers below 10 tend to form pores [45]. The second general rule is that longer surfactants with $i + j \geq 18$ can undergo a buckling instability [33]. In terms of spontaneous curvature, C18E10 was expected to form bumps because it has an HLB number of 12.7. C16E2 and C18E2 were expected to form pores with HLB numbers of 5.2 and 5.6, respectively. C6E2 and C12E4 have roughly neutral curvature with HLB = 10. In terms of buckling, C16E2, C18E2, and C18E10 are sufficiently large to undergo this instability, but it appeared to be suppressed due to the small film thickness.

Although these rules guided our choice of surfactants, the outcomes did not match the predictions in all cases. Deviations are not uncommon, but the small thickness of the films and relatively short self-assembly time chosen for

this study were somewhat near the extreme values for these particular parameters. They were somewhat atypical in that respect, and the resulting surfaces might not therefore obey the general rule. The thickness and self-assembly time were held constant for each sample to remain consistent, but they could have just as easily been chosen to create a more typical surface morphology. Note that these particular surfaces are not meant to represent a systematic change in surface structure, but rather to demonstrate that simply changing the surfactant and no other variable is sufficient to generate a wide variety of surface morphologies.

We then examined the effects of these nano-, micro-, and multiscaled topographies on phenotypic changes in ASCs. In stromal/stem cells, these structural differences are detected as changes in mechanical cues and are relayed to the nucleus where they are transduced into changes in gene expression [46,47]. Consequently, changes in surface features affect stromal/stem cell lineage specification. The complexity of the signaling cascade makes it somewhat challenging, however, to discern what specific cues are directing cell behavior. Dalby *et al.*, found that increased 'randomness' of surface features affected osteogenic differentiation of bone marrow-derived mesenchymal stem cells [48]. Though the current study was limited in its investigation of mechanistic components such as genetic and protein markers, future studies will aim to identify which specific features act as guidance cues and probe the underlying pathways.

The three surfaces that stimulated increased calcium deposition relative to the flat surfaces are C12E4, C16E2, and C6E2. Two of the three surfaces were identified as having a hierarchy of nanoscale bumps superimposed over larger pores or ridges. Although the C12E4 surface primarily had mico-scale ridges, the SEM and optical profilometry data in Figure 2 reveal some nanoscale roughness that may have been sufficient to qualify as a distinct hierarchical level. Interestingly, cells grown on these same three surfaces appeared less spread out compared to cells on control (flat) surfaces as well as C18E10 and C18E2 after just one day of culture. Specifically, the cell bodies of ASCs grown on C12E4, C16E2, and C6E2 appear more compact with long, thin filopodia compared to the broader, spread morphologies of cells on other surfaces. Quantitative assessments suggest a negative correlation between cell area and the extent of mineral deposition, a finding that has also been reported by other groups investigating the effects of topographies on cells [49,50]. Future studies will aim to assess various metrics of cell shape such as aspect ratio and expand the parameters to a wider range of surfactants to help shed light on the correlation. Promising surfaces such as C16E2 will be studied in depth by modulating surface parameters such as feature size and determining the resultant effects on cell growth and differentiation.

Mounting evidence suggests that hierarchical guidance cues direct the development and functional properties of the nervous [51,52], skeletal [53], and circulatory systems [54]. The FLA technique has great potential to create such hierarchical topographies. In this proof-of-concept study, we demonstrate that topographical surfaces generated by this self-assembly process may be able to modify cellular behavior indicating that FLA-generated hierarchical topography can result in changes in proliferation and osteogenic differentiation relative to a flat surface. In this study, osteogenic differentiation of ASCs on FLA surfaces was assessed with biochemical stimulation since the default pathway for ASCs is not osteoblast formation. In future studies, a more systematic investigation of topographical structures with quantifiable hierarchy will be used to systematically determine its impact on ASC growth and differentiation. By modulating for various levels of hierarchical formation, future studies may also pinpoint the effects of the absence or presence of specific features, enabling FLA to be guided by design.

## 5. CONCLUSIONS

This study demonstrated that the novel FLA technique can generate a diverse array of hierarchical topographic features, ranging from simple bumps and pores to complex ridges. Moreover, these features and combinations thereof may be easily designed and controlled by the manipulation of simple experimental parameters such as self-assembly time and film thickness. The resultant surfaces are non-cytotoxic and highly reproducible at a fraction of the cost of surfaces produced using conventional techniques, while achieving a complexity and biomimicry that makes FLA particularly pertinent for use in investigating the effects of nanotopography on cells. Our experiments illustrate that, applied to cell culture, FLA surfaces are not only able to maintain cell viability and growth but can elicit differences in proliferation and osteogenic differentiation of ASCs, suggesting that the technology may be amenable to bone tissue engineering applications. The data also provides preliminary suggestions that FLA may be an effective means for studying the ability of multi-scale topographical features to influence stem cell fate. Future studies will refine the functionality and manufacture of FLA, expand the library of generated surfaces, and further explore the effects of hierarchy and specific features in cell growth and differentiation. In particular, future emphasis will be placed on analyzing the mechanistic rationale for cell responses and using this to design ideal topographies in 3D structures such as scaffolds. In turn, this might provide useful insights and innovative applications of the FLA technique in the fields of tissue engineering and regenerative medicine.

***Acknowledgements:*** *This work was supported by grants from the Maryland Stem Cell Research Fund, (2014-13 MSCRF-0699), the NSF CAREER award (1350554) and the Johns Hopkins Center for Musculoskeletal Research to WLG. JJB acknowledges partial support for this work from the Hafstad Fellowship provided through The Johns Hopkins University Applied Physics Laboratory. We acknowledge the kind support of Dr. Jeffrey Gimble who provided ASCs for this study.*

## 5. REFERENCES

[1] Cui YL, Qi AD, Liu WG, Wang XH, Wang H, Ma DM, *et al.* Biomimetic surface modification of poly (L-lactic acid) with chitosan and its effects on articular chondrocytes in vitro. *Biomaterials* 2003;24:3859-3868.

[2] Ishii D, Yabu H, Shimomura M. Novel biomimetic surface based on a self-organized metal− polymer hybrid structure. *Chemistry of Materials* 2009;21:1799-1801.

[3] Shin H, Jo S, Mikos AG. Biomimetic materials for tissue engineering. *Biomaterials* 2003;24:4353-4364.

[4] Kulangara K, Leong KW. Substrate topography shapes cell function. *Soft Matter* 2009;5:4072-4076.

[5] Curtis A, Wilkinson C. Topographical control of cells. *Biomaterials* 1997;18:1573-1583.

[6] Dunn G, Heath J. A new hypothesis of contact guidance in tissue cells. *Experimental cell research* 1976;101:1-14.

[7] Anselme K, Bigerelle M. Role of materials surface topography on mammalian cell response. *International Materials Reviews* 2011;56:243-266.

[8] Anselme K, Ponche A, Bigerelle M. Relative influence of surface topography and surface chemistry on cell response to bone implant materials. Part 2: biological aspects. *Proceedings of the Institution of Mechanical Engineers, Part H: Journal of Engineering in Medicine* 2010;224:1487-1507.

[9] Lord MS, Foss M, Besenbacher F. Influence of nanoscale surface topography on protein adsorption and cellular response. *Nano Today* 2010;5:66-78.

[10] Watt FM, Huck WTS. Role of the extracellular matrix in regulating stem cell fate. *Nat Rev Mol Cell Biol* 2013;14:467-473.

[11] Hoffman-Kim D, Mitchel JA, Bellamkonda RV. Topography, cell response, and nerve regeneration. *Annual review of biomedical engineering* 2010;12:203-231.

[12] Yoon H, Ahn SH, Kim GH. Three-Dimensional Polycaprolactone Hierarchical Scaffolds Supplemented with Natural Biomaterials to Enhance Mesenchymal Stem Cell Proliferation. *Macromolecular Rapid Communications* 2009;30:1632-1637.

[13] Sefcik LS, Neal RA, Kaszuba SN, Parker AM, Katz AJ, Ogle RC, *et al.* Collagen nanofibres are a biomimetic substrate for the serum-free osteogenic differentiation of human adipose stem cells. *J Tissue Eng Regen Med* 2008;2:210-220.

[14] Shi Z, Neoh KG, Kang ET, Poh CK, Wang W. Enhanced endothelial differentiation of adipose-derived stem cells by substrate nanotopography. *Journal of tissue engineering and regenerative medicine* 2014;8:50-58.

[15] Young PS, Tsimbouri PM, Gadegaard N, Meek RM, Dalby MJ. Osteoclastogenesis/osteoblastogenesis using human bone marrow-derived cocultures on nanotopographical polymer surfaces. *Nanomedicine* 2015;10:949-957.

[16] Seras-Franzoso J, Tsimbouri PM, Burgess KV, Unzueta U, Garcia-Fruitos E, Vazquez E, Topographically targeted osteogenesis of mesenchymal stem cells stimulated by inclusion bodies attached to polycaprolactone surfaces. *Nanomedicine* 2014;9:207-220.

[17] Mendonça G, Mendonça DBS, Aragão FJL, Cooper LF. Advancing dental implant surface technology – From micron- to nanotopography. *Biomaterials* 2008;29:3822-3835.

[18] Oh S, Brammer KS, Li YJ, Teng D, Engler AJ, Chien S, *et al.* Stem cell fate dictated solely by altered nanotube dimension. *Proceedings of the National Academy of Sciences* 2009;106:2130-2135.

[19] Bettinger CJ, Langer R, Borenstein JT. Engineering substrate topography at the micro-and nanoscale to control cell function. *Angewandte Chemie International Edition* 2009;48:5406-5415.

[20] Le Guehennec L, Soueidan A, Layrolle P, Amouriq Y. Surface treatments of titanium dental implants for rapid osseointegration. *Dental materials : official publication of the Academy of Dental Materials* 2007;23:844-854.

[21] Pennisi CP, Zachar V, Gurevich L, Patriciu A, Struijk J. The influence of surface properties of plasma-etched polydimethylsiloxane (PDMS) on cell growth and morphology. Engineering in Medicine and Biology Society (EMBC), 2010 Annual International Conference of the IEEE: *IEEE*; 2010. p. 3804-3807.

[22] Ito T, Okazaki S. Pushing the limits of lithography. *Nature* 2000;406:1027-1031.

[23] Okazaki S. Resolution limits of optical lithography. Journal of Vacuum Science & Technology B: Microelectronics and Nanometer Structures 1991;9:2829-2833.

[24] Dalby MJ, McCloy D, Robertson M, Agheli H, Sutherland D, Affrossman S, *et al.* Osteoprogenitor response to semi-ordered and random nanotopographies. *Biomaterials* 2006;27:2980-2987.

[25] Dalby MJ, Riehle MO, Sutherland DS, Agheli H, Curtis AS. Changes in fibroblast morphology in response to nano-columns produced by colloidal lithography. *Biomaterials* 2004;25:5415-5422.

[26] Martins A, Chung S, Pedro AJ, Sousa RA, Marques AP, Reis RL, *et al.* Hierarchical starch-based fibrous scaffold for bone tissue engineering applications. *Journal of Tissue Engineering and Regenerative Medicine* 2009;3:37-42.

[27] Benkoski JJ, Jones RL, Douglas JF, Karim A. Photocurable oil/water interfaces as a universal platform for 2-D self-assembly. *Langmuir* 2007;23:3530-3537.

[28] Benkoski JJ, Hu H, Karim A. Generation of hierarchical topologies from photocrosslinkable, particle-stabilized emulsions. *Macromolecular Rapid Communications* 2006;27:1212-1216.

[29] Morris ML, Baird LM, Panigrahi A, Gross MC, Deacon RM, Benkoski JJ. Surfactant sculpting of biologically inspired hierarchical surfaces. *Soft Matter* 2013;9:9857-9866.

[30] Rydholm AE, Bowman CN, Anseth KS. Degradable thiol-acrylate photopolymers: polymerization and degradation behavior of an in situ forming biomaterial. *Biomaterials* 2005;26:4495-4506.

[31] Rodriguez A-M, Pisani D, Dechesne CA, Turc-Carel C, Kurzenne J-Y, Wdziekonski B, *et al.* Transplantation of a multipotent cell population from human adipose tissue induces dystrophin expression in the immunocompetent mdx mouse. *Journal of Experimental Medicine* 2005;201:1397-1405.

[32] Opperhuizen A, Damen HW, Asyee GM, Van Der Steen JM, Hutzinger O. Uptake and elimination by fish of polydimethylsiloxanes (silicones) after dietary and aqueous exposure. *Toxicological & Environmental Chemistry* 1987;13:265-285.

[33] Van Gestel C, Otermann K, Canton J. Relation between water solubility, octanol/water partition coefficients, and bioconcentration of organic chemicals in fish: A review. *Regulatory Toxicology and Pharmacology* 1985;5:422-431.

[34] Zitko V. Metabolism and distribution by aquatic animals. Reactions and Processes: *Springer*; 1980. p. 221-229.

[35] Annelin R, Frye C. The piscine bioconcentration characteristics of cyclic and linear oligomeric permethylsiloxanes. *Science of the total environment* 1989;83:1-11.

[36] Bruggeman W, Weber-Fung D, Opperhuizen A, VanDerSteen J, Wijbenga A, Hutzinger O. Absorption and retention of polydimethylsiloxanes (silicones) in fish: preliminary experiments. *Toxicological & Environmental Chemistry* 1984;7:287-296.

[37] Benkoski JJ, Morris ML, Panigrahi A, Deacon RM, Chan P. Surfactant sculpting of photocurable monomers into hierarchically organized biomimetic materials. *Abstr Pap Am Chem S* 2012;243.

[38] Kim EJ, Boehm CA, Mata A, Fleischman AJ, Muschler GF, Roy S. Post microtextures accelerate cell proliferation and osteogenesis. *Acta biomaterialia* 2010;6:160-169.

[39] Kumar D, Gittings JP, Turner IG, Bowen CR, Hidalgo-Bastida LA, Cartmell SH. Polarization of hydroxyapatite: influence on osteoblast cell proliferation. *Acta biomaterialia* 2010;6:1549-1554.

[40] Ng KW, Leong DT, Hutmacher DW. The challenge to measure cell proliferation in two and three dimensions. *Tissue engineering* 2005;11:182-191.

[41] Quent VM, Loessner D, Friis T, Reichert JC, Hutmacher DW. Discrepancies between metabolic activity and DNA content as tool to assess cell proliferation in cancer research. *Journal of cellular and molecular medicine* 2010;14:1003-1013.

[42] Brammer KS, Choi C, Frandsen CJ, Oh S, Johnston G, Jin S. Comparative cell behavior on carbon-coated TiO2 nanotube surfaces for osteoblasts vs. osteo-progenitor cells. *Acta biomaterialia* 2011;7:2697-2703.

[43] Hu J, Feng K, Liu X, Ma PX. Chondrogenic and osteogenic differentiations of human bone marrow-derived mesenchymal stem cells on a nanofibrous scaffold with designed pore network. *Biomaterials* 2009;30:5061-5017.

[44] Correia C, Bhumiratana S, Yan LP, Oliveira AL, Gimble JM, Rockwood D, *et al.* Development of silk-based scaffolds for tissue engineering of bone from human adipose-derived stem cells. *Acta biomaterialia* 2012;8:2483-2492.

[45] Israelachvili JN. The science and applications of emulsions - an overview *Colloids and Surfaces* 1994;91:1-8.

[46] Guilak F, Cohen, D.M., Estes, B.T., Gimble, J.M., Liedtke, W., Chen, C.S. Control of Stem Cell Fate by Physical Interactions with the Extracellular Matrix. *Cell Stem Cell* 2009;5:17 - 26.

[47] Hung BP, Hutton, D.L., Grayson, W.L. Mechanical control of tissue-engineered bone. *Stem Cell Research and Therapy* 2013;4:10- 6.

[48] Dalby MJ, Gadegaard N, Tare R, Andar A, Riehle MO, Herzyk P, *et al.* The control of human mesenchymal cell differentiation using nanoscale symmetry and disorder. *Nature materials* 2007;6:997-1003.

[49] Kaivosoja E, Myllymaa S, Takakubo Y, Korhonen H, Myllymaa K, Konttinen YT, *et al.* Osteogenesis of human mesenchymal stem cells on micro-patterned surfaces. *J Biomater Appl* 2013;27:862-871.

[50] Myllymaa S, Kaivosoja E, Myllymaa K, Sillat T, Korhonen H, Lappalainen R, *et al.* Adhesion, spreading and osteogenic differentiation of mesenchymal stem cells cultured on micropatterned amorphous diamond, titanium, tantalum and chromium coatings on silicon. *J Mater Sci-Mater M* 2010;21:329-341.

[51] Britland S, Perridge C, Denyer M, Morgan H, Curtis A, Wilkinson C. Morphogenetic guidance cues can interact synergistically and hierarchically in steering nerve cell growth. *Experimental Biology Online* 1997;1:1-15.

[52] Wadsworth WG, Hedgecock EM. Hierarchical guidance cues in the developing nervous system of C. elegans. *BioEssays : news and reviews in molecular, cellular and developmental biology* 1996;18:355-362.

[53] Oyen ML. The materials science of bone: Lessons from nature for biomimetic materials synthesis. *MRS bulletin* 2008;33:49-55.

[54] Parker KK, Ingber DE. Extracellular matrix, mechanotransduction and structural hierarchies in heart tissue engineering. *Philos Trans R Soc Lond B Biol Sci* 2007;362:1267-1279.

## SAŽETAK

**Novi proces samo-organizacije površinski aktivnih supstanci za dobijanje podloga sa topografskim karakteristikama na više dužinskih skala za gajenje i diferentovanje matičnih ćelija**

Eric G. Xie[1,2], Colin A. Cook[1,2], Warren L. Grayson[1-3], Jason J. Benkoski[4]

[1]*Translational Tissue Engineering Center, Johns Hopkins University, Baltimore MD, USA*
[2]*Department of Biomedical Engineering, Johns Hopkins University, Baltimore MD, USA*
[3]*Department of Material Sciences and Engineering, Johns Hopkins University, Baltimore MD, USA*
[4]*Johns Hopkins University Applied Physics Laboratory, Research and Exploratory Development Department, Laurel, MD, USA*

(Naučni rad)

Topografske karakteristike podloge mogu kontaktom značajno da utiču na metabolizam i diferentovanje matičnih ćelija. Iako je odgovor matičnih ćelija na topografske karakteristike na nano-, mikro- i mezo-nivou široko izučavan, malo se zna o uzajamnom dejstvu karakteristika površine koje deluju simultano na više dužinskih skala. Ograničavajući faktor je dostupnost efikasnih metoda velikog kapaciteta za ispitivanje potencijalno neograničenog parametarskog prostora. U ovom radu je opisana jednostavna metoda za brzo generisanje hijerarhije topografskih karakteristika na više dužinskih skala na polimernim podlogama primenom samo-organizacije površinski aktivnih supstanci na granici faza monomer/voda. U ranijim ispitivanjima smo poli(dimetilsiloksan)-diakrilat (PDMS-DA) oblikovali u vidu površina koje imitiraju morfologije više tkiva, dok je u ovoj studiji metoda usavršena kako bi se dobile biokompatibilne podloge. Radi upravljanja velikim brojem mogućih vrednosti parametara, opseg ove studije je ograničen na karakteristike površine dužinskih skala od nanometarskih (< 1 μm) do mikrometarskih dimenzija (1-50 μm) i to pojedinačno ili u kombinaciji. Matične ćelije izolovane iz masnog tkiva su zasejane na pet tipova podloga i gajene u kontrolnom odnosno osteogenom medijumu nakon čega su analizirane u pogledu morfologije, proliferacije i diferentovanja u pravcu osteogenih ćelija. Uočene su statistički značajne razlike u pogledu odgovora ćelija na različite podloge. Jedan od rezultata je pokazao povećanu osteogenu diferencijaciju ćelija gajenih na podlogama sa topografskim karakteristikama nano-veličina na neravninama mikro-dimenzija, što ukazuje da takva hijerarhijska struktura pospešuje osteogene karakteristike površine.

*Ključne reči*: samo-organizacija; topografija; matične ćelije izolovane iz masnog tkiva; inženjerstvo tkiva kosti; poli(dimetilsiloksan)